

Multiplicity-dependent saturation momentum in p -Pb collisions at 5.02 TeVTakeshi Osada **Department of Natural Sciences, Faculty of Science and Engineering,
Tokyo City University, Tamazutsumi 1-28-1, Setagaya-ku, Tokyo 158-8557, Japan*

(Received 3 November 2020; revised 13 January 2021; accepted 2 February 2021; published 22 February 2021)

Semi-inclusive transverse momentum spectra observed in proton-proton and proton-lead nuclear collisions at LHC energies obey a geometric scaling with a scaling variable using multiplicity-dependent saturation momentum. The saturation momentum extracted from the experimental data is proportional to the 1/6 power of the hadron multiplicity in the final state. However, the system's transverse size is proportional to the 1/3 power of the multiplicity, and the saturation momentum and the transverse size of the system are strongly correlated with the hadron multiplicity in the final state. Since the saturation momentum is proportional to the average transverse momentum of hadrons, one predicts average transverse momentum is also proportional to the 1/6 power of the multiplicity, which is consistent with experimental results at the LHC energy. It is also found that a nuclear modification factor R_{pPb} calculated by the multiplicity-dependent saturation momentum decreases in $p_T \lesssim 1$ GeV/c and that the R_{pPb} 's behavior thought to be caused by nuclear shadowing can partially explained. However, Cronin enhancement experimentally observed at $2 \lesssim p_T \lesssim 6$ GeV/c is not reproduced. However, the experimental result, including the Cronin effect, can be reproduced well by introducing p_T dependence as at most 4–5% correction to the multiplicity-dependent saturation momentum. The relationship between the geometric scaling in the semi-inclusive distributions and the string percolation model is also discussed.

DOI: [10.1103/PhysRevC.103.024911](https://doi.org/10.1103/PhysRevC.103.024911)**I. INTRODUCTION**

The gluon saturation picture [1–4] has provided us with many hints for a unified understanding of multiparticle production in which strong interactions play a significant role. For example, in a color glass condensate (CGC) model [5,6] which is an effective theory to describe saturated gluons with small x , the saturation scale [7,8] separates the classical gluon field into fast frozen color sources and slow dynamical color fields. The existence of the intrinsic scale of the transverse momentum $Q_s(x)$ is a crucial underlying assumption of the effective theory. Furthermore, by replacing p_T in a Bjorken x of the saturation scale $Q_s(x)$ with some constant characteristic one, one can introduce the energy-dependent saturated momentum $Q_{\text{sat}}(W)$, which depends only on the collision energy W . Then, it is a unique scale that governs p_T spectra of the produced particles, and as a result, geometric scaling [9–11] (GS) is emerges. The authors of Refs. [12–16] confirmed GS certainly holds for inclusive p_T spectra of high-energy pp , pA , and AA collisions.

In the previous works [17,18], it has been confirmed that GS also holds even for semi-inclusive distributions. In those works, the authors introduced a saturation momentum $Q_{\text{sat}}(W^*)$ that depends on the effective energy W^* , which has a one-to-one correspondence with the observed multiplicity in the final state instead of the initial colliding energy W . In this article, I will discuss based on a perspective that the physics

of gluon saturation is a fundamental property and should serve as a comprehensive explanation of multiparticle production in different reaction types, energies, and multiplicities.

Recently, a collective motion thought to be characteristic of the hadronic matter produced by the collisions of large systems such as AA has been found in high-multiplicity events by small systems such as pp and pA collisions [19,20]. Therefore, another hint to the unified understanding of multiparticle production in any type of reaction would be seen the similarity in high multiplicity events of pp and pA collisions. Among the observables that depend on various multiplicities, the multiplicity dependence on the mean transverse momentum in pp , pA , and AA collisions is impressive because their dependence is significantly different for each reaction type [21]. In particular, theoretical studies need to explain a result that the multiplicity dependence on the mean transverse momentum of p -Pb collisions is weaker than that of pp for $dn/dy \gtrsim 20$.

The so-called cold nuclear matter effects found in pA collisions has been investigated by experiments at RHIC [22–24] and LHC energies [25–27], and theoretical explanations have been added to those results [28–30]. An important observable, nuclear modification factor R_{pA} , is defined by a ratio of the p_T spectrum of pA collisions to that of pp collisions, with particular attention paid to the increase in the yield of p -Pb collisions known as the Cronin effect [31–33]. One may consider the deviation of the value of R_{pA} from 1 as the nuclear matter effects on particle production, making it possible to investigate the multiple scattering effects in the nuclear medium including nuclear shadowing [34] and transverse momentum broadening [35]. One may also extract information on the

*t-osada@tcu.ac.jp

small x gluon distribution of a nucleus in the early stage of collisions [36]. The CGC formalism has been successful in explaining these nuclear shadowing, and transverse momentum broadening in pA collisions at the LHC [37]. For collisions of different system sizes, such as pA , two saturation momentum scales, i.e., Q_s^p for proton and Q_s^A for nucleus, are introduced into theoretical models. However, due to less constrained the initial value of those saturation scales, it gives theoretical uncertainties of the nuclear modification factor R_{pA} at LHC [38]. It has also been pointed out that fluctuations in protons' saturation momentum play a significant role in the multiplicity distribution of produced particles in pA collisions [39].

In this paper, the multiplicity-dependent saturation momentum is extracted using the geometric scaling property of the semi-inclusive p_T spectra in pp and p -Pb collisions. Furthermore, using the experimental results on the nuclear modification factor in the central rapidity region, the saturation momentum that governs the multiparticle production process in p -Pb collisions is investigated.

This article is organized as follows. It is briefly explain that the geometric scaling for the semi-inclusive distribution and determine its parameters in Sec. II. Besides, by fitting a universal function of GS to the semi-inclusive p_T spectra observed in pp and p -Pb collisions at LHC energies, the multiplicity-dependent saturation momentum $Q_{\text{sat}}(W^*)$ and the effective interaction radius R_T^* are determined as a function of the multiplicity density in the central rapidity region. Then, it is shown that the experimental results on the multiplicity dependence of $\langle p_T \rangle$ are consistent with the GS's conjecture in Sec. III. In the Sec. IV, the role of the saturation momentum in the nuclear modification factor R_{pPb} is clarified by comparing the present model calculations using $Q_{\text{sat}}(W^*)$ obtained for pp and p -Pb, respectively. Section V contains the summary and some concluding remarks.

II. GS IN SEMI-INCLUSIVE TRANSVERSE MOMENTUM SPECTRA

Consider transverse momentum spectra of pp or p -Pb collisions with colliding (center of mass) energy W classified by the multiplicity of the charged hadrons in its final state. In the following formulation of the model based on GS with using semi-inclusive spectra, except for a determination part of the multiplicity-dependent saturation momentum and the universal functions, I follow the theoretical formulation developed in Refs. [17,18] for pp collisions.

For each event multiplicity classes, the semi-inclusive transverse spectra of hadrons normalized by a effective crosssectional reaction area S_T^* can be scaled to an universal function

$$\frac{1}{S_T^*} \frac{1}{2\pi p_T} \frac{d^2 n_{\text{ch}}}{dp_T dy} = \mathcal{F}(\tau), \quad (1a)$$

with a scaling variable

$$\tau^{1/(2+\lambda)} \equiv \frac{p_T}{Q_{\text{sat}}(W^*)}, \quad (1b)$$

instead of the merely transverse momentum p_T . Here, $Q_{\text{sat}}(W^*)$ denotes a multiplicity-dependent saturation mo-

mentum as a function of the effective energy W^* [17,18]. Equation (1a) is originally for the gluon p_T distribution based on the saturation picture [4,7,40]. It is assumed that the local parton-duality [41] holds in good approximation, and then hadron spectra observed have the same as a gluon distribution but different total multiplicity. The factor of the effective area S_T^* absorbs the ratio of the partons and hadrons' multiplicity as a constant. For an inclusive distribution, the saturation momentum (in literature, it is often referred to as an average saturation momentum or an energy-dependent saturation momentum),

$$Q_{\text{sat}}(W) = Q_0 \left(\frac{x_0 W}{Q_0} \right)^{\lambda/(\lambda+2)}, \quad (2)$$

is uniquely determined by collision energy W with constants $x_0 = 1.0 \times 10^{-3}$, $Q_0 = 1.0$ GeV/ c , $\lambda = 0.22$ [14,42]. In our previous work [18], which deals with GS for the semi-inclusive spectrum, one determines W^* and S_T^* as fitting parameters to the semi-inclusive spectra for each multiplicity fixed by the event class. Therefore, $Q_{\text{sat}}(W^*)$ has a one-to-one correspondence with the multiplicity and regarded as a function of the multiplicity. Here, multiplicity-dependent saturation momentum $Q_{\text{sat}}(W^*)$ is assumed to have the same energy dependence as that of Eq. (2), and it is a saturation momentum in which W in Eq. (2) is just replaced by W^* .

In the present model, S_T^* and W^* are fitting parameters, which is equivalent to searching for S_T^* and $Q_{\text{sat}}(W^*)$ directly. In fact, there is the following relationship between W^* and Q_{sat} :

$$W^* = \frac{Q_{\text{sat}}}{x_0} \left(\frac{Q_{\text{sat}}}{Q_0} \right)^{2/\lambda}. \quad (3)$$

The function \mathcal{F} in Eq. (1a) is called universal function, and Tsallis type function is often used in GS [14]:

$$\mathcal{F}(\tau) = \left[1 + (q-1) \frac{\tau^{1/(2+\lambda)}}{\kappa} \right]^{-1/(q-1)}, \quad (4)$$

where q is a so-called nonextensive parameter and κ is a constant parameter which connects $Q_{\text{sat}}(W^*)$ as an intermediate energy scale and hadronization energy scale, freeze-out temperature, for example. In previous analyses, $Q_{\text{sat}}(W^*)$ was determined by assuming that a universal function for the inclusive spectra and that for the semi-inclusive spectra are the same. However, the p_T spectra broadens for the high multiplicity events at 7.0 and 13.0 TeV pp collisions. (This tendency already can be seen in Fig. 2 of Ref. [18].) Therefore, in this paper, only π^\pm spectra are used to exclude particles with large masses that may be sensitive in the large p_T region. One can also consider light hadrons such as pions to be more suitable for the assumption, such as the saturation picture of gluons and the subsequent particle production in the central rapidity.

Since the saturation picture can be universally applied to gluons inside highly relativistic contracted hadronic or nuclear matter, GS holds regardless of the collision system and it can be valid in high-energy pp and p -Pb collisions. Therefore, one needs to find $Q_{\text{sat}}(W^*)$ and S_T^* so that the semi-inclusive

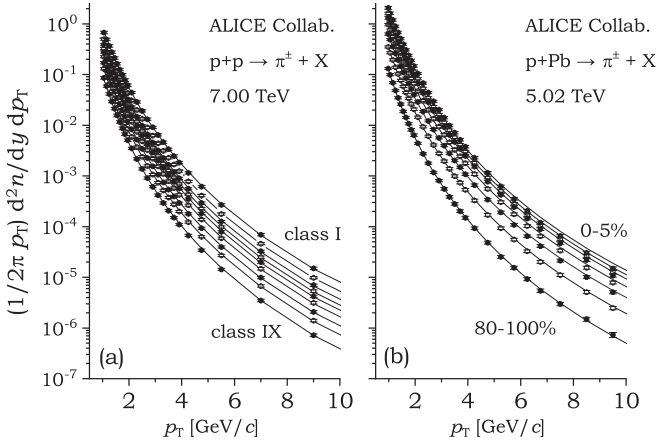


FIG. 1. Fit results of $S_T^* \mathcal{F}$ to the semi-inclusive spectra for (a) pp collisions at energy 7.00 TeV [43] (the multiplicity class is from I (top) to IX (bottom), and the class X is omitted because the multiplicity is too small). (b) The same as panel (a) but for p -Pb collisions at energy 5.02 TeV [44,48] [the multiplicity class is from 0–5% (top) to 80–100% (bottom)]. The value of $q = 1.145$ and $\kappa = 0.1100$ of the universal function \mathcal{F} of Eq. (4) is used. For the multiplicity of each class, the values of $Q_{\text{sat}}(W^*)$ and S_T^* are extracted from these fits.

distribution observed in pp and p -Pb collisions becomes a common universal function $\mathcal{F}(\tau)$. In Fig. 1, two examples of the fit to the semi-inclusive spectra with $q = 1.145$, $\kappa = 0.1100$ are shown for $p + p \rightarrow \pi^\pm + X$ at energy $W = 7.00$ TeV and for $p + \text{Pb} \rightarrow \pi^\pm + X$ at energy $W = 5.02$ TeV observed by ALICE Collaboration [43,44]. Besides, Fig. 2 shows that 67 semi-inclusive distributions (947 data points), including the spectra shown in Fig. 1, observed in $\sqrt{s} = W = 2.76, 7.00, 13.0$ TeV pp collisions [43,45,46], and $W = 5.02$ TeV p -Pb collisions [44,47,48] almost perfectly scale to the universal function (1a) with $q = 1.145$ and $\kappa = 0.1100$ (see also Table I).

As shown in Fig. 2, one can find suitable $Q_{\text{sat}}(W^*)$ and an effective radius of the interaction area $R_T^* \equiv \sqrt{S_T^*/\pi}$ to scale the semi-inclusive p_T spectra of both pp and p -Pb collisions to the same universal function $\mathcal{F}(\tau)$. Figures 3(a) and 4(a) show $Q_{\text{sat}}(W^*)$ and R_T^* extracted from the semi-inclusive p_T spectra, respectively. Both $Q_{\text{sat}}(W^*)$ and R_T^* are functions of the multiplicity dn_π/dy of the final state pion in the central rapidity region. It should be noted that $Q_{\text{sat}}(W^*)$ and R_T^* are mutually correlated quantities because they are subject to the fixed multiplicity constraint of the semi-inclusive event as the

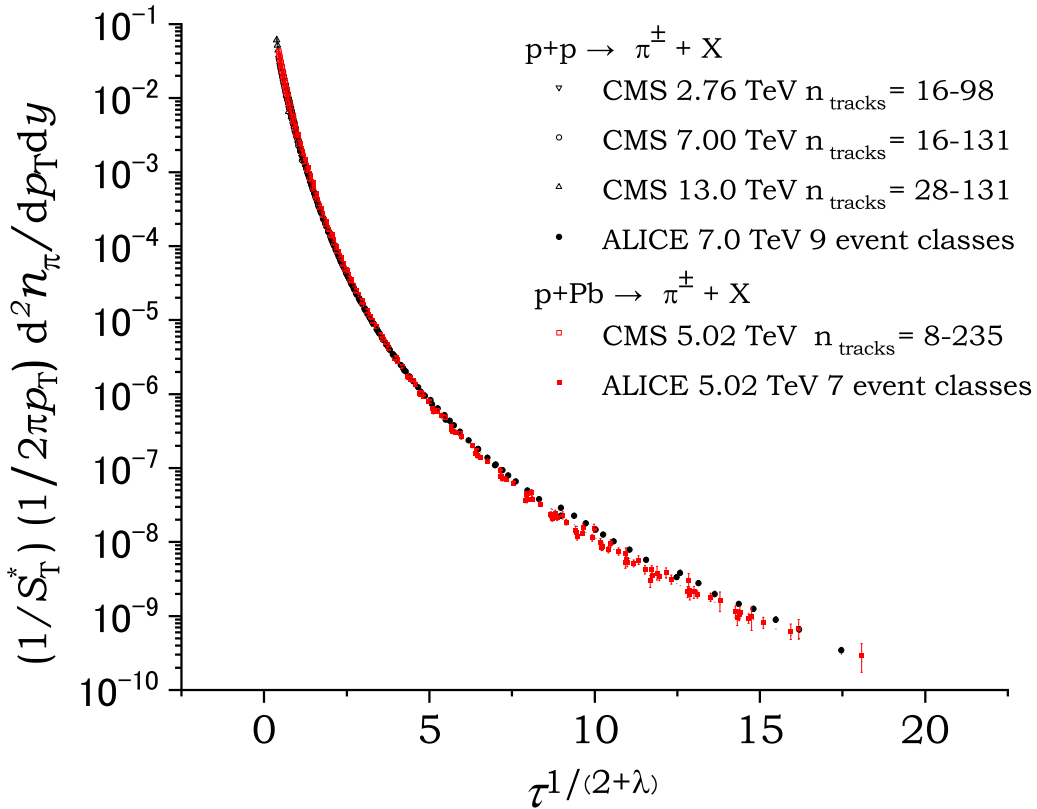


FIG. 2. Geometric scaling of the semi-inclusive p_T spectra in pp collisions (black symbols) for multiplicity class with track number $16 \leq n_{\text{tracks}} \leq 98$ at $\sqrt{s}=2.76$ TeV, $16 \leq n_{\text{tracks}} \leq 131$ at $\sqrt{s}=7.00$ TeV [45], and $28 \leq n_{\text{tracks}} \leq 172$ at $\sqrt{s}=13.0$ TeV [46] by CMS Collaboration (the pseudorapidity window $|\eta| < 2.4$). The p_T spectra in pp collisions for nine event classes with multiplicity range of $3.98 \leq dn_{\text{ch}}/dy \leq 20.1$ at 7.00 TeV [43] by ALICE Collaboration are also shown. For p -Pb collisions (red symbols) at 5.02 TeV for multiplicity class with track number $19 \leq n_{\text{tracks}} \leq 235$ by CMS [47] and ALICE Collaboration seven event classes with multiplicity range of $4.4 \leq dn_{\text{ch}}/dy \leq 45$ [44,48] are shown.

TABLE I. Values of q and κ in the universal function Eq. (4) of geometrical scaling.

Analysis	Observable	q	κ	$\tau^{1/(2+\lambda)}$
pp incl [18]	Charged	1.134	0.1292	<40
pp incl	π^\pm	1.132	0.1111	<2.5
pp incl	$\pi^\pm + K^\pm$	1.129	0.1211	<2.5
pp, p -Pb semi-incl	π^\pm	1.145	0.1100	<18

following:

$$\frac{dn_\pi}{dy} = \frac{2\pi\kappa^2}{(2-q)(3-2q)} S_T^* Q_{\text{sat}}^2(W^*). \quad (5)$$

Considering that $R_T^* \propto [dn_\pi/dy]^{1/3}$ approximately holds as well known in the observation of the HBT effects [49–51], the saturation momentum should be proportional to the 1/6 power of the multiplicity, $Q_{\text{sat}}(W^*) \propto [dn_\pi/dy]^{1/6}$. Actually, when $Q_{\text{sat}}(W^*)$ and R_T^* are plotted by $[dn_\pi/dy]^{1/6}$ and $[dn_\pi/dy]^{1/3}$, respectively, one confirms such dn/dy dependence as shown in Figs. 3(b) and 4(b), which is consistent with the simple conjecture expected from GS.

Let me discuss here the rather peculiar multiplicity dependence on $Q_{\text{sat}}(W^*)$ extracted from p_T spectra of p -Pb collisions at 5.02 TeV observed by the ALICE Collaboration [44]. It is observed that the saturation momentum extracted from the spectra is significantly less multiplicity-dependent than the case of pp collisions. However, the extraction of $Q_{\text{sat}}(W^*)$ from spectra observed by CMS Collaboration [47] with the same collision system and the same energy gives almost the same results as that obtained in pp collisions. While ALICE Collaboration has published data on the transverse momentum spectra for $p_T < 20$ GeV/c, it is used for $0.6 < p_T < 3.0$ GeV/c to rule out hadron jet effects in the extraction of $Q_{\text{sat}}(W^*)$ in this analysis. Choosing the maximum $p_T = 2.0$ GeV/c, which is the same as the CMS,

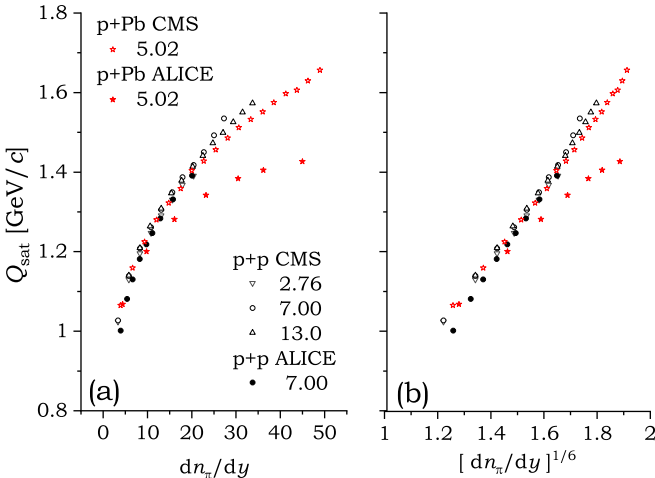


FIG. 3. (a) The multiplicity-dependent saturation momentum $Q_{\text{sat}}(W^*)$ obtained by the fitting Eq. (1) to the semi-inclusive π^\pm transverse spectra as a function of dn_π/dy . (b) The same as panel (a) but as a function of $[dn_\pi/dy]^{1/6}$.

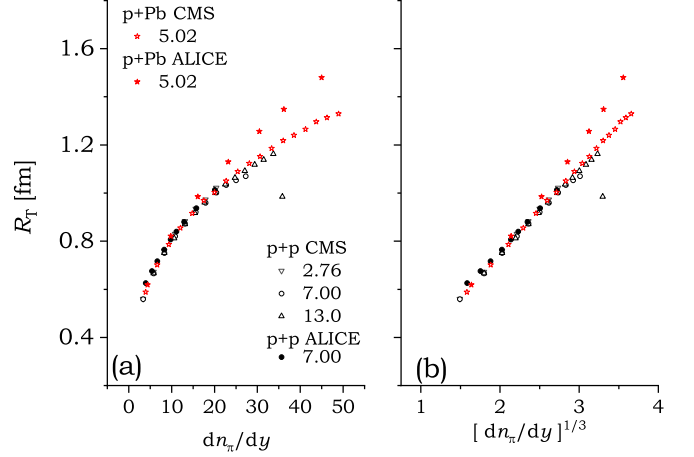


FIG. 4. (a) Effective transverse radii R_T^* of interaction cross sectional area obtained by the fitting Eq. (1) to the semi-inclusive π^\pm transverse spectra as a function of dn_π/dy . (b) The same as panel (a) but as a function of $[dn_\pi/dy]^{1/3}$.

did not significantly affect results obtained. However, the rapidity range is slightly different between two collaborations, where CMS is $|y| < 1$, whereas ALICE is $0 < y < 0.5$, and ALICE has observed pions for the more central rapidity region. It is still unclear whether the rapidity window of the semi-inclusive p_T spectra affects the evaluation of $Q_{\text{sat}}(W^*)$ and R_T^* .

The $Q_{\text{sat}}(W^*)$ and R_T^* shown in Figs. 3(a) and 4(a) are obtained by the following fitting formulas of 1/6 and 1/3 power of dn_π/dy , respectively:

$$Q_{\text{sat}}(W^*) = a_Q + b_Q \left(\frac{dn_\pi}{dy} \right)^{\frac{1}{6}}, \quad (6a)$$

$$R_T^* = a_R + b_R \left(\frac{dn_\pi}{dy} \right)^{\frac{1}{3}}. \quad (6b)$$

The values of the coefficients $a_Q, b_Q, a_R,$ and b_R fitted to the data of Figs. 3(a) and 4(a) are shown in Table II. Here, if the constant terms a_Q and a_R can be ignored, then the following relation is derived from Eq. (5):

$$\sqrt{\frac{(2-q)(3-2q)}{2\pi^2}} = \frac{\kappa b_Q b_R}{0.197 [\text{GeV fm}]}. \quad (7a)$$

As shown in Table II, Eq. (7a) is approximately satisfied by the LHC energies of pp and p -Pb collisions. At the initial stage of collisions, gluon number density saturates due to their nonlinear interactions. The inverse of saturation momentum $1/Q_{\text{sat}}$ gives a transverse cross-sectional size scale where saturated gluons are packed (one may consider it as a color flux tube size) [7,17,53]. If the tube size scale were evaluated from inclusive spectra, it would be determined solely by the collision energy W and not depend on the event multiplicity. For example, when the collision energy is $W = 7.0, 13.0$ TeV, the saturation momentum is $Q_{\text{sat}}(W) = 1.213$ and 1.289 GeV/c, respectively. (These give flux tube size scale 0.162 and 0.153 fm, respectively.) However, the saturation momentum obtained from the semi-inclusive spectra

TABLE II. The values of the parameters used in Eqs. (6a) and (6b) for fitting $Q_{\text{sat}}(W^*)$ and R_T^* extracted from the semi-inclusive p_T spectra, respectively. The right- and left-hand sides of Eq. (7a) are also shown to check the GS conjecture.

		$a_Q + b_Q(dn/dy)^{1/6}$		$a_R + b_R(dn/dy)^{1/3}$		Eq. (7a)	
		a_Q	b_Q	a_R	b_R	l.h.s.	r.h.s.
$pp \rightarrow \pi^\pm + X$							
2.76 TeV [45]	$-1.0 < y < 1.0$	-0.019	0.854	0.006	0.371	0.175	0.177
7.00 TeV [45]	$-1.0 < y < 1.0$	-0.149	0.954	0.051	0.345	0.175	0.184
7.00 TeV [43]	$-0.5 < y < 0.5$	-0.225	0.985	0.073	0.345	0.175	0.190
13.0 TeV [46]	$-1.0 < y < 1.0$	-0.472	1.164	0.156	0.302	0.175	0.196
$pp \rightarrow h^\pm + X$							
5.02 TeV [52]	$-0.8 < \eta < 0.8$	-0.311	1.160	0.078	0.296	0.181	0.211
13.0 TeV [52]	$-0.8 < \eta < 0.8$	-0.390	1.323	0.072	0.246	0.181	0.200
$p\text{-Pb} \rightarrow \pi^\pm + X$							
5.02 TeV [47]	$-1.0 < y < 1.0$	0.078	0.899	0.030	0.358	0.175	0.180
5.02 TeV [44]	$0.0 < y < 0.5$	0.315	0.600	-0.130	0.446	0.175	0.149

is larger than that from the inclusive case especially in the high multiplicity event class. Therefore, it is considered that the size of the flux tube that appears in the initial stage of collision becomes smaller and shrinks slightly as the gluon multiplicity increases. As a result, the tube size appears as a multiplicity dependence such as $1/Q_{\text{sat}}(W^*) \propto [dn/dy]^{-1/6}$; see Fig. 5(a). However, since the reaction cross-sectional area S_T^* becomes large as $S_T^* \propto [dn/dy]^{2/3}$, one expects the number of flux tubes in the area S_T^* to be precisely proportional to dn/dy . In fact, Fig. 5(b) shows that the number of color flux tubes packed in the effective reaction area, $n_{tb} = S_T^* Q_{\text{sat}}^2(W^*)$, extracted from the pp and $p\text{-Pb}$ semi-inclusive events increases linearly from $dn_\pi/dy \gtrsim 20$. Since the size of the color flux tube can be evaluated as $1/Q_{\text{sat}}$, one gets the number of particles produced from a tube per unit rapidity as follows:

$$\frac{1}{n_{tb}} \frac{dn}{dy} \approx \frac{2\pi\kappa^2}{(2-q)(3-2q)} = \left[\frac{0.197[\text{GeV fm}]}{b_Q b_R} \right]^2. \quad (7b)$$

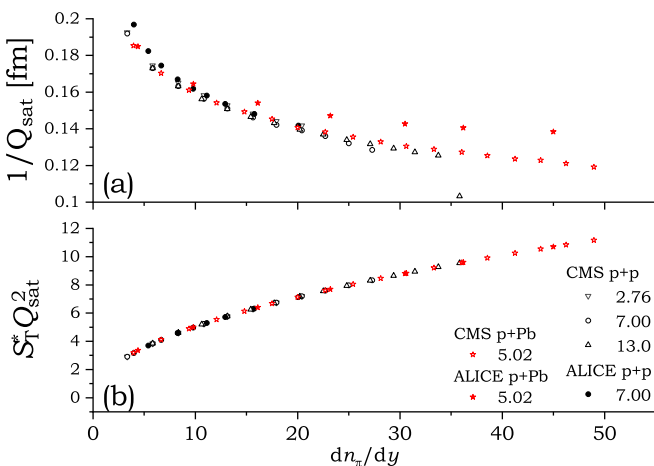


FIG. 5. dn/dy dependence of (a) $1/Q_{\text{sat}}(W^*)$, which can be interpreted as a scale of the radius of color flux tube, and (b) $S_T^* Q_{\text{sat}}^2(W^*)$, which is the total number of the tubes produced in the interaction area.

Based on the flux tube picture, the above equation near the central rapidity region does not depend on rapidity.

Let us return to the discussion of the rather peculiar $Q_{\text{sat}}(W^*)$ and R_T^* behavior found in $p\text{-Pb}$ collisions. The change in the slope of $Q_{\text{sat}}(W^*)$ and R_T^* in Figs. 3 and 4 observed by ALICE for $p\text{-Pb}$ collisions at 5.02 TeV indicates that these b_Q and b_R changes. Therefore, it can be considered that the event multiplicity-dependence of both the flux tube size and the gluon interaction radius changes at $[dn/dy]^{1/6} \approx 1.6$. Before closing this section, let us analyze the transverse momentum spectrum obtained by the $p\text{-Pb}$ collision [44] in two parts. One is the soft part, $0.5 \leq p_T \leq 1.5$ GeV/c (soft π^\pm), and the other is the hard part, $3.0 \leq p_T \leq 19$ GeV/c (hard π^\pm). By fitting data of each p_T window, the saturation momentum $Q_{\text{sat}}(W^*)$ can be extracted and compared to investigate the relationship with the effect of jet quenching [54]. [Since the measurement range of CMS Collaboration is $p_T \leq 1.175$ GeV/c, it is classified as soft π^\pm , and the result is the same as a result shown in Fig. 3(b).] The multiplicity dependence of $Q_{\text{sat}}(W^*)$ obtained in these two p_T windows are shown in Fig. 6. The multiplicity dependence of the saturation momentum obtained from soft π^\pm is not much different from results shown in Fig. 3(b) for low multiplicities. However, for high multiplicity, one observes that Q_{sat} is more clearly proportional to the 1/6 power of the multiplicity. For hard π^\pm , the multiplicity dependence is the same as the soft π^\pm case up to $[dn/dy]^{1/6} \approx 1.75$, but Q_{sat} is suppressed in a higher multiplicity. These results may indicate the formation of thin color flux tubes is suppressed by some reason in the initial state, or gluons (or pions) with high transverse momentum emitted from thin color flux tubes are suppressed due to interactions with hot hadronic matter or cold nuclear matter.

III. MEAN p_T IN SEMI-INCLUSIVE EVENTS

The different dn/dy dependence on the average transverse momentum ($\langle p_T \rangle$) between pp and $p\text{-Pb}$ collisions has been reported in Ref. [21]. In GS model, since the average transverse momentum of the charged hadrons is proportional to the multiplicity-dependent saturation momentum $Q_{\text{sat}}(W^*)$, one expects $\langle p_T \rangle$ also proportional to the 1/6 power of the

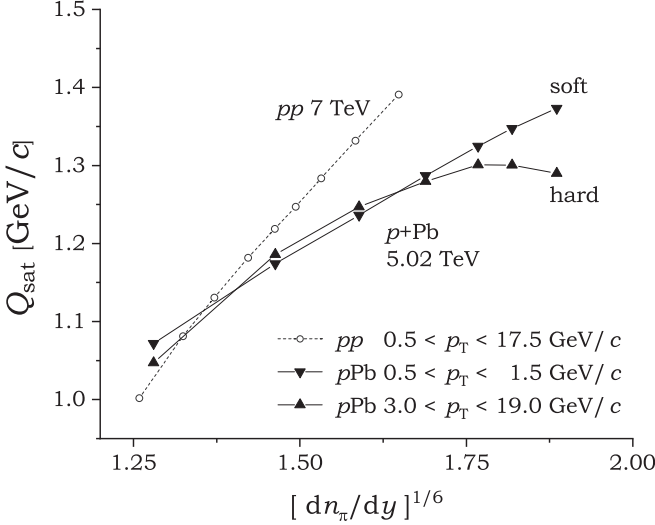


FIG. 6. The multiplicity dependence of the saturation momentum Q_{sat} obtained by fitting Eq. (1) to the semi-inclusive transverse momentum distribution in p -Pb collisions for soft p_T part ($0.5 \leq p_T \leq 1.5$ GeV/c) and hard p_T part ($3.0 \leq p_T \leq 19$ GeV/c). For reference purposes, saturation momenta Q_{sat} obtained by pp collisions at 7.0 TeV are shown.

multiplicity [17,18]:

$$\langle p_T \rangle = \frac{2\kappa Q_{\text{sat}}(W^*)}{4-3q} \propto \left(\frac{dn}{dy} \right)^{1/6}. \quad (8)$$

Experimental data on the mean transverse momentum of π^\pm observed by CMS and charged hadron h^\pm observed by ALICE are replotted in Fig. 7 as a function of dn/dy to the 1/6 power. As shown in Fig. 7, the experimental results are substantially proportional to the 1/6 power of multiplicity. It

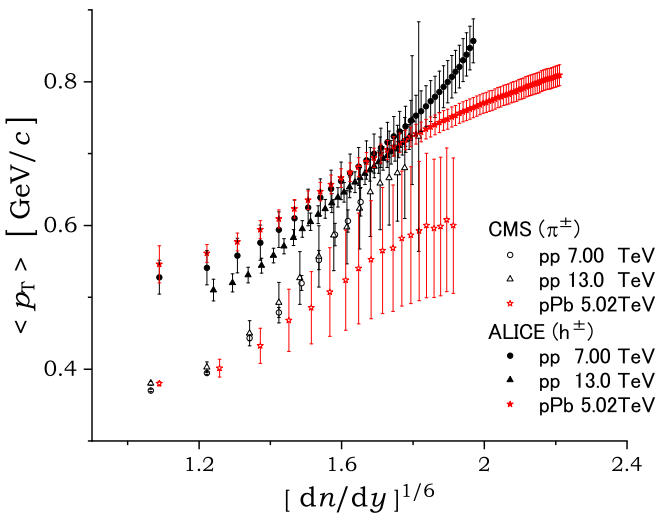


FIG. 7. Mean transverse momentum $\langle p_T \rangle$ of a charged hadron or charged pion as a function of 1/6 power of dn/dy . The data on the multiplicity dn/dy dependence of $\langle p_T \rangle$ of charged hadrons observed by ALICE Collaboration [21,52] and the data on charged pions observed by CMS Collaboration [45–47].

is worth noting that the multiplicity dependence of $\langle p_T \rangle$ for p -Pb data observed by the two experimental groups shows similar changes around $[dn/dy]^{1/6} \approx 1.6$ ($dn/dy \approx 20$), although the absolute value of it differs due to the difference in acceptance of the measurement. These experimental facts suggest that the multiplicity dependence of $Q_{\text{sat}}(W^*)$ changes at $dn/dy \approx 20$ in central rapidity region. Here, ignoring the contribution from a_Q and a_R in Eq. (6) as small and using Eqs. (7a) and (8), one obtains the following for the slope of the graph shown in Fig. 7:

$$\begin{aligned} \frac{\langle p_T \rangle}{[dn/dy]^{1/6}} &= \frac{0.197 [\text{GeV fm}] \sqrt{2(2-q)(3q-2)}}{b_R \pi(4-3q)} \\ &= \frac{2\kappa b_Q}{4-3q} \approx 0.3 - 0.4 [\text{GeV/c}]. \end{aligned} \quad (9)$$

The multiplicity dependence of $\langle p_T \rangle$ given by Eq. (9) well explain the behavior of the experimental results. Moreover, one may explain the behavior of $\langle p_T \rangle$ for p -Pb collisions observed by ALICE Collaboration for $[dn/dy]^{1/6} \gtrsim 1.6$ is due to the change of behavior of the $Q_{\text{sat}}(W^*)$. Namely, the decrease of b_Q and the increase of b_R (see Table II) change the slope of $\langle p_T \rangle$ vs $[dn/dy]^{1/6}$. Note that there is no change in the proportionality relationship to the 1/6 power of multiplicity, just a change in the coefficients. As pointed out in Sec. II, the saturation momentum $Q_{\text{sat}}(W^*)$ extracted from the semi-inclusive p_T spectra in p -Pb collisions changes its slope at $[dn/dy]^{1/6} \gtrsim 1.6$ [see Fig. 3(b)]. Interestingly, both $Q_{\text{sat}}(W^*)$ and $\langle p_T \rangle$ show a qualitative change around the almost same dn/dy in their multiplicity dependence. Thus, the saturation momentum that governs the p_T spectra increases in proportion to the 1/6 power of multiplicity with the same proportional coefficient for low multiplicity events in both pp and p -Pb collisions. However, for high multiplicity events in p -Pb collisions, b_Q extracted from the ALICE data changes its value at $[dn/dy]^{1/6} \approx 1.6$. Furthermore, as can be seen from Fig. 4, the coefficient of $[dn/dy]^{1/3}$ for R_T^* also changes at the same multiplicity as $Q_{\text{sat}}(W^*)$. This is precisely what Eq. (9) expresses. However, for pp collisions, there are no indications that the multiplicity dependence of $\langle p_T \rangle$ changes up to the maximum multiplicity observed.

This multiplicity dependence change in $\langle p_T \rangle$ may be interpreted as follows. As can be seen from Fig. 5(b), the number of flux tubes is proportional to the event multiplicity regardless of the reaction and energy. (Approximately four pions are produced per unit rapidity from one color flux tube.) In the case of pp , the multiplicity increases as the tube's diameter decrease simultaneously as the system's reaction size increases. (More tubes are packed in the interaction area.) In p -Pb collisions, the multiplicity is increased by the same mechanism as the pp collision when the multiplicity is small. However, at a certain multiplicity, the flux tube's size becomes difficult to become thin, and instead, the reaction region becomes large, so that the multiplicity increases.

IV. NUCLEAR MODIFICATION FACTOR

In this paper, to introduce the multiplicity dependence of the saturation momentum, the originally existing p_T

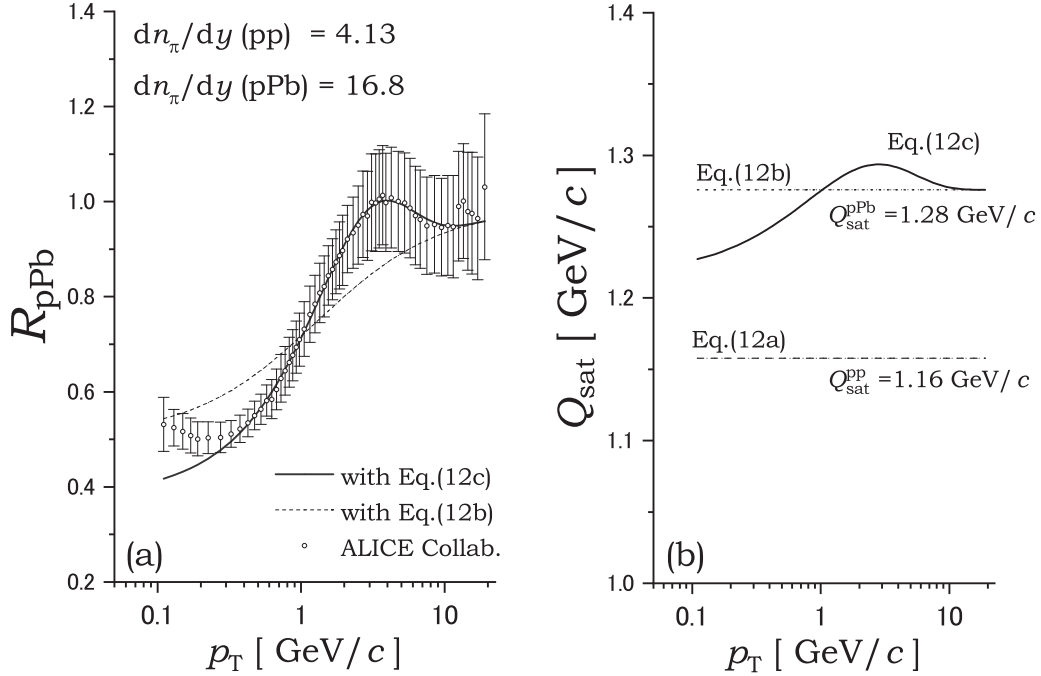


FIG. 8. (a) Comparison of the nuclear modification factor (10b) with ALICE data for p -Pb collision at 5.02 TeV. The saturation momenta used for pp [given by Eq. (12a)] and p -Pb collisions [given by Eq. (12b) or Eq. (12c)] are shown in panel (b).

dependence of the saturation momentum has been neglected by replacing it with a representative p_T , i.e., $Q_{\text{sat}}(W^*)$. If the nuclear modification factor does not include any final-state interactions, then it may be the observable where the transverse momentum dependence ignoring so far is most pronounced. Therefore, it should be evaluated how much transverse momentum dependence is required for the obtained saturated momentum as a correction by comparing it with the available experimental data.¹

In Sec. II, it is confirmed that the semi-inclusive p_T spectra of both pp and p -Pb collisions scale to the same universal function. The saturation momentum, which plays a central role in the GS, behaves differently from pp , especially in high-multiplicity events of p -Pb collisions. In the case of p -Pb collisions, nuclear matter may affect the multiplicity-dependent saturation momentum. To investigate the nuclear matter effects on the saturation momentum in p -Pb collisions, the nuclear modification factor experimentally observed is compared with the present model. The modification factor is a ratio of p_T differential yield relative to the pp reference and it is defined by [48]

$$R_{\text{pPb}}^{\text{exp}}(p_T) = \frac{d^2 N_{\pi}^{\text{pPb}}/d\eta dp_T}{\langle T_{\text{pPb}} \rangle d^2 \sigma_{\text{ch}}^{\text{pp}}/d\eta dp_T}, \quad (10a)$$

where $\langle T_{\text{pPb}} \rangle = 0.0983 \text{ mb}^{-1}$ [48] is an average nuclear overlap function. In experiments, $R_{\text{pPb}}^{\text{exp}}$ is defined by the inclusive

¹The experimental data for nuclear modification factors are obtained using inclusive transverse momentum spectra, including various multiplicities events. Therefore, it is necessary to compare the data on the nuclear correction factors using semi-inclusive events with the present model for a more accurate discussion.

spectra, but it is substituted with the following equation using the semi-inclusive spectra to clarify the role of the saturation momentum:

$$R_{\text{pPb}}(p_T) = \frac{d^2 n_{\pi}^{\text{pPb}}/dy dp_T}{C d^2 n_{\text{ch}}^{\text{pp}}/dy dp_T}. \quad (10b)$$

Here, C in Eq. (10b) is a constant factor and is related to the experimental data of $\langle T_{\text{pPb}} \rangle$ and the total inelastic nucleon-nucleon cross section $\sigma_{\text{INEL}}^{\text{NN}} = 67.6 \text{ mb}$ [55] as follows:

$$C = \langle T_{\text{pPb}} \rangle \sigma_{\text{INEL}}^{\text{NN}} = 6.645. \quad (11)$$

The multiplicity of semi-inclusive events for pp and p -Pb collisions is applied by those of the average multiplicity of inclusive events, respectively: i.e., $\frac{dn_{\pi}^{\text{pPb}}}{dy} \approx \langle \frac{dN_{\pi}^{\text{pPb}}}{d\eta} \rangle = 16.81$ [56] and $\frac{dn_{\pi}^{\text{pp}}}{dy} \approx \langle \frac{dN_{\pi}^{\text{pp}}}{d\eta} \rangle = 4.13$ [55]. Therefore, by Eq. (6a) with values appearing in Table II, one obtains

$$Q_{\text{sat}}^{\text{pp}}(W^*) = 1.158 \text{ GeV}/c, \quad (12a)$$

$$Q_{\text{sat}}^{\text{pPb}}(W^*) = 1.276 \text{ GeV}/c. \quad (12b)$$

The nuclear modification factor R_{pPb} calculated by Eqs. (12a) and (12b) for the multiplicity-dependent saturation momentum of pp and p -Pb collisions, respectively, is shown by the broken line in Fig. 8(a). One can partially reproduce R_{pPb} , such as suppression in the low p_T region and asymptotic behavior in the high p_T region. However, the simple calculation using Eqs. (12a) and (12b) overestimates R_{pPb} in the low p_T region compared to the experimental data and cannot reproduce the so-called Cronin enhancement.

Let us introduce p_T dependence as a phenomenological side effect on the saturation momentum $Q_{\text{sat}}(W^*)$, which has been regarded as a function of effective energy W^* (or average

TABLE III. The values of the parameters used in Eq. (12d) giving $R_{pPb}(p_T)$ (solid curve) in Fig. 8.

$d\bar{n}_\pi^{pPb}/dy$	$d\bar{n}_{ch}^{pp}/d\eta$	α	β	γ	χ^2/dof
16.8	4.13	6.05	0.886	1.56	1.13/46

multiplicity dn/dy) only. Recall that the saturation momentum $Q_{\text{sat}}(W)$ is derived from an intermediate energy scale $Q_s^2(x) \equiv Q_0^2(x_0/x)^\lambda$ given by Bjorken $x = p_T/W$. Then Q_{sat} is defined with the solution p_T satisfying $p_T = Q_s^2(p_T/W)$. Therefore, this is a good approximation for $p_T \approx Q_{\text{sat}}$ and neglects the weak p_T dependence in $p_T \gg Q_{\text{sat}}$ and $p_T \ll Q_{\text{sat}}$ region, resulting in deviations from the original intermediate energy scale $Q_s(x)$ (see Fig. 1 in Ref. [18]). This weak p_T dependence may need to be taken into account, especially for observables such as Eq. (10b), which is sensitive to the behavior of p_T . Another reason to introduce this effect is to investigate the gluon recombination effect, which determines the scale of saturation momentum in multiparticle production from experimental data. (Of course, it is not possible to distinguish whether recombination occurred before or after the color flux tube formation.) Therefore, I introduce such an effect to analysis of data and investigate whether it contributes to explaining R_{pPb}^{exp} obtained [48]. Thus, instead of Eq. (12b), a possible $Q_{\text{sat}}^{pPb}(W^*)$ may be given by the following:

$$Q_{\text{sat}}^{pPb}(W^*) = a_Q + b_Q \left[\frac{dn_\pi^{pPb}}{dy} + \delta \right]^{1/6}, \quad (12c)$$

where

$$\delta = \alpha \left(\frac{p_T - \beta Q_{\text{sat}}^{pp}}{Q_{\text{sat}}^{pp}} \right) \exp \left[\frac{-p_T}{\gamma Q_{\text{sat}}^{pp}} \right]. \quad (12d)$$

The solid line in Fig. 8(a) shows a fitting result of Eq. (10b) with Eqs. (11) and (12) to the experimental data $R_{pPb}^{\text{exp}}(p_T)$. The values of the parameters used in Eq. (12d) are also shown in Table III. As shown in Fig. 8(b), one can well reproduce the experimental data of the nuclear modification factor by introducing at most about 4% change for saturation momentum $p_T \lesssim 20$ GeV/c. In particular, the Cronin effect, in which an enhancement peak appears around $p_T = 2\text{--}6$ GeV/c in R_{pPb}^{exp} , is explained by being about 1% larger than the multiplicity-dependent saturation momentum of p -Pb, Eq. (12b). Note that the original saturation scale $Q_s(x)$ with fixed collision energy W depends on the power of the gluon's transverse momentum; $Q_s(x) \propto p_T^{-\lambda/2}$. For example, when comparing the value of the saturation scale at $p_T \approx 1$ GeV/c and 5 GeV/c, the value at 5 GeV/c is about 15% smaller than the value at $p_T \approx 1$ GeV/c. Hence, the direction of the correction that reintroduces the weak p_T dependence of $Q_s(x)$ is the opposite direction of the correction required to explain the experimental result of R_{pPb}^{exp} .

There are two possibilities to explain this variation in the saturation momentum $Q_{\text{sat}}(W^*)$. One possibility is that the p_T dependence in saturation momentum may be explained as the effects of interactions such as absorption and emission of gluons after flux tubes decay. The other is that such fluctuation may have already existed around the average saturation

momentum at the time the color flux tube was formed. The former suggests that the application of parton-hadron duality requires caution. It may be possible to study these two possibilities by similar analyzing a nuclear modification factor by using prompt photons [57] in the same way as discussed in this article.

V. SUMMARY AND CONCLUDING REMARKS

Semi-inclusive spectra of pp and p -Pb collisions normalized by the 1/3 power of the multiplicity scales to the same universal function using a saturation momentum proportional to the 1/6 power of the multiplicity. The agreement between the experimental results and GS conjecture suggests that the saturation momentum, determined by a multiplicity of the final state (by assuming local parton hadron duality, it also depends on the gluon's initial state) dominates the multiparticle production regardless of the reaction type and collision energy. The existence of geometric scaling across different reactions such as proton-proton and proton-nucleus collisions strongly suggests the gluon saturation mechanism in the early stage of the reaction, which should be a physics common to the elementary processes of phenomena on the multiparticle production. One of the advantages of GS analysis is that one can derive information on color flux tube formation in the early stage of hadronic or nuclear collisions from the multiplicity-dependent saturation momentum $Q_{\text{sat}}(W^*)$. The information may be carried by the coefficients b_Q and b_R in Eqs. (6a) and (6b). Moreover, there is a constraint condition between them as Eqs. (7) or (9). Based on a color flux tube picture with these equations, one can point out a reason why the multiplicity dependence of mean transverse momentum at high multiplicity in p -Pb collisions varies compared to pp collisions is a change of the multiplicity dependence of the diameter of the color flux tube and the size of the area packed tubes. Furthermore, observations of the nuclear modification factor may suggest that the multiplicity-dependent saturation momentum needs to introduce small transverse momentum dependence. However, the physical origin of this correction for the multiplicity-dependent saturation momentum is still unclear.

The string percolation model [58–61] has clear correspondence with the geometric scaling [62] examined in detail in this paper. Before closing this last section, let us consider why the multiplicity dependence of saturation momentum differs between pp and p -Pb collisions using the string percolation model. Consider N color strings packed into a region S_T produced by pp or p -Pb collisions; given the cross-sectional area $\sigma_1 = \pi r_0^2$ of one string and the string density $\eta = N\sigma_1/S_T$ in the area S_T , the average number of effective strings $\langle N \rangle$ is given by the following (see Appendix):

$$\langle N \rangle = S_T \frac{(1 - e^{-\eta})}{\pi r_0^2 F(\eta)}, \quad (13)$$

where $F(\eta)$ is a color reduction factor

$$F(\eta) = \sqrt{\frac{1 - e^{-\eta}}{\eta}}. \quad (14)$$

By noting that $\langle N \rangle \approx S_T Q_{\text{sat}}^2$, the corresponding saturation momentum is given by

$$Q_{\text{sat}}^2 \propto \begin{cases} \sqrt{\eta} & \text{for } \eta \gg 1, \\ \eta & \text{for } \eta \ll 1. \end{cases} \quad (15)$$

It is also interesting to note that if S_T is proportional to the 2/3 power of multiplicity, $\sqrt{\eta}$ (for the case of low multiplicity case) is proportional to the 1/6 power of multiplicity, which is consistent with the conclusion reached in this paper.

In the string percolation model, the multiplicity dependence of the saturation momentum (the dependence of the inverse of the effective string radius) is explained as a function of the string density η . Therefore, the obtained results that the multiplicity dependence of the saturation momentum in pp and p -Pb is different for high multiplicity events suggest that the string densities are substantially different in pp and p -Pb when the multiplicity is sufficiently large. The result that the multiplicity dependence of saturation momentum is different for pp and p -Pb collisions, and smaller for p -Pb compared to pp , suggests that the color field overlap is larger for p -Pb than for pp when comparing events of the same multiplicity. It can also be understood that the transverse reaction area S_T with the same multiplicity as pp is larger for p -Pb, since the number of the effective string is decrease due to the string fusion.

The suggestion that there are more overlapping strings in p -Pb than in pp may be naturally attributed to the effect of nucleons existing around the reaction region that are not present in the case of pp . The color flux tubes (effective strings) may be excited by (or interact with) the surrounding nuclear matter, which increases the string density.

The next step may be to analyze the semi-inclusive p_T spectrum obtained from AA collisions to determine a multiplicity-dependent saturation momentum. Furthermore, the multiplicity dependence of the mean transverse momentum of Pb-Pb collisions is even weaker than that of p -Pb [21]. It needs to investigate whether multiplicity-dependent saturation momentum extracted from the AA collisions also satisfies the 1/6 power law of the multiplicity and clarify the difference between p -A and AA from the viewpoint of a multiplicity-dependent saturation momentum. I plan to investigate those issues at some other opportunity.

ACKNOWLEDGMENT

This work was supported by JSPS KAKENHI Grant No. 20K03978.

APPENDIX: STRING PERCOLATION MODEL

Suppose that after high-energy pp or p -Pb collisions, N strings are generated and packed into the cross-sectional area S . Furthermore, suppose the cross-sectional area of each string is given by $\sigma_1 = \pi r_0^2$, and the multiplicity generated from one string is μ_1 . When n strings overlap in an area S_n , the color fields in that area are must be summed up like a vector. Therefore, the multiplicity of hadrons generated from the overlapped n strings is not proportional to n but to \sqrt{n} . Then, the multiplicity produced in the region $S = \sum_n S_n$ is as

follows [61]:

$$\mu = \sum_{n=1}^N \frac{\sqrt{n} S_n}{\sigma_1} \mu_1. \quad (A1)$$

However, the mean-squared transverse momentum must be summed like a scalar:

$$\langle p_T^2 \rangle = \frac{N \mu_1}{\mu} \langle p_T^2 \rangle_1 = \frac{N \langle p_T^2 \rangle_1}{\sum_{n=1}^N \sqrt{n} S_n / \sigma_1}. \quad (A2)$$

In the limit of $N, S \rightarrow \infty$, assuming that the probability of finding the region of n strings form a cluster, $p(n) = S_n/S$, obeys the Poisson distribution with the mean value

$$\eta \equiv N \sigma_1 / S = \left(\frac{r_0^2}{R^2} \right) N, \quad (A3)$$

the multiplicity of the final state is as follows:

$$\mu = \frac{S}{\sigma_1} \sum_{n=1}^{\infty} \frac{\sqrt{n} \eta^n}{n!} e^{-\eta} \mu_1. \quad (A4)$$

Therefore, the color reduction factor $F(\eta)$, which is defined by the reduction rate of multiplicity due to the fusion of strings, is given by

$$F(\eta) \equiv \frac{\mu}{N \mu_1} = \frac{1}{\eta} \sum_{n=1}^{\infty} \sqrt{n} \frac{\eta^n e^{-\eta}}{n!} \approx \sqrt{\frac{1 - e^{-\eta}}{\eta}}. \quad (A5)$$

From Eq. (A2), the mean-squared transverse momentum is given by

$$\langle p_T^2 \rangle = \frac{\langle p_T^2 \rangle_1}{F(\eta)}. \quad (A6)$$

Note here that $\sigma_1 F(\eta)$ can be interpreted as the cross-sectional area of the effective string, which may be equivalent to the flux tubes in the Glasma picture, formed in the color electric field. Hence, the area occupied by the stings $S - S_0$ divided by the area of the effective string $\sigma_1 F(\eta)$ gives the average number of effective strings (the average number of color tubes):

$$\langle N \rangle = \frac{S - S_0}{\sigma_1 F(\eta)} = \frac{R^2 (1 - e^{-\eta})}{r_0^2 F(\eta)}. \quad (A7)$$

Here, noting the correspondence between the effective string and the color flux tube in the Glass picture, one obtains

$$\langle N \rangle = \pi R^2 \frac{(1 - e^{-\eta})}{\pi r_0^2 F(\eta)} \rightarrow S_T Q_{\text{sat}}^2. \quad (A8)$$

Thus, the saturation momentum is related to the string mean density, and one also gets

$$Q_{\text{sat}}^2 = \frac{\sqrt{\eta (1 - e^{-\eta})}}{\pi r_0^2}. \quad (A9)$$

Hence, one can confirm from Eq. (A8) that the saturation momentum Q_{sat} certainly depends on the multiplicity of the final state hadrons through the string density η , and the behavior changes as follows, depending on whether η is large or small:

$$Q_{\text{sat}}^2 \propto \begin{cases} \sqrt{\eta} & \text{for } \eta \gg 1, \\ \eta & \text{for } \eta \ll 1. \end{cases} \quad (A10)$$

- [1] Y. V. Kovchegov and E. Levin, *Quantum Chromodynamics at High Energy*, Vol. 33 (Cambridge University Press, Cambridge, UK, 2012).
- [2] L. V. Gribov, E. M. Levin, and M. G. Ryskin, *Phys. Rep.* **100**, 1 (1983).
- [3] J. P. Blaizot and A. H. Mueller, *Nucl. Phys. B* **289**, 847 (1987).
- [4] D. Kharzeev and M. Nardi, *Phys. Lett. B* **507**, 121 (2001).
- [5] E. Iancu, A. Leonidov, and L. McLerran, in *QCD Perspectives on Hot and Dense Matter. Proceedings of the NATO Advanced Study Institute, Summer School, Cargese, France, August 6–18, 2001* (Kluwer Academic, Dordrecht, Netherlands, 2002), pp. 73–145.
- [6] J.-P. Blaizot and F. Gelis, *Nucl. Phys. A* **750**, 148 (2005), Quark gluon plasma. New discoveries at RHIC: A case of strongly interacting quark gluon plasma. Proceedings of the RBRC Workshop, Brookhaven, Upton, USA, May 14–15, 2004.
- [7] D. Kharzeev and E. Levin, *Phys. Lett. B* **523**, 79 (2001).
- [8] F. Gelis, E. Iancu, J. Jalilian-Marian, and R. Venugopalan, *Ann. Rev. Nucl. Part. Sci.* **60**, 463 (2010).
- [9] A. M. Stasto, K. J. Golec-Biernat, and J. Kwiecinski, *Phys. Rev. Lett.* **86**, 596 (2001).
- [10] E. Iancu, K. Itakura, and L. McLerran, *Nucl. Phys. A* **708**, 327 (2002).
- [11] E. Iancu, K. Itakura, and L. McLerran, *Nucl. Phys. A* **721**, C293 (2003), Particles and nuclei. Proceedings of the 16th International Conference, PANIC'02, Osaka, Japan, September 30–October 4, 2002.
- [12] M. Praszalowicz, *Phys. Rev. Lett.* **106**, 142002 (2011).
- [13] M. Praszalowicz, *Phys. Lett. B* **727**, 461 (2013).
- [14] L. McLerran and M. Praszalowicz, *Phys. Lett. B* **741**, 246 (2015).
- [15] M. Praszalowicz and A. Francuz, *Phys. Rev. D* **92**, 074036 (2015).
- [16] M. Praszalowicz, *Acta Phys. Polon. Suppl.* **8**, 399 (2015), Proceedings of the International Meeting of Excited QCD 2015: Tatranska Lomnica, Slovakia, March 8–14, 2015.
- [17] T. Osada and M. Ishihara, *J. Phys. G* **45**, 015104 (2018).
- [18] T. Osada and T. Kumaoka, *Phys. Rev. C* **100**, 034906 (2019).
- [19] R. Preghenella, EPJ Web Conf. 171, 11003 (2018), Proceedings of the 17th International Conference on Strangeness in Quark Matter (SQM 2017) Utrecht, the Netherlands, July 10–15, 2017.
- [20] V. Khachatryan *et al.* (CMS collaboration), *Phys. Lett. B* **765**, 193 (2017).
- [21] B. B. Abelev *et al.* (ALICE collaboration), *Phys. Lett. B* **727**, 371 (2013).
- [22] A. Adare *et al.* (PHENIX collaboration), *Phys. Rev. C* **88**, 024906 (2013).
- [23] C. Aidala *et al.* (PHENIX collaboration), *Phys. Rev. C* **99**, 044912 (2019).
- [24] C. Aidala *et al.* (PHENIX collaboration), *Phys. Rev. C* **101**, 034910 (2020).
- [25] B. Abelev *et al.* (ALICE collaboration), *Phys. Rev. Lett.* **110**, 082302 (2013).
- [26] J. Adam *et al.* (ALICE collaboration), *Phys. Rev. C* **91**, 064905 (2015).
- [27] V. Khachatryan *et al.* (CMS collaboration), *J. High Energy Phys.* **04** (2017) 039.
- [28] A. Rezaeian and Z. Lu, *Nucl. Phys. A* **826**, 198 (2009).
- [29] A. H. Rezaeian, *Proceedings of the Europhysics Conference on High energy physics (EPS-HEP 2009): Cracow, Poland, July 16–22, 2009* (PoS, 2009), p. 45.
- [30] A. Dumitru, D. E. Kharzeev, E. M. Levin, and Y. Nara, *Phys. Rev. C* **85**, 044920 (2012).
- [31] J. Cronin, H. J. Frisch, M. Shochet, J. Boymond, R. Mermod, P. Piroue, and R. L. Sumner, *Phys. Rev. D* **11**, 3105 (1975).
- [32] D. Kharzeev, Y. V. Kovchegov, and K. Tuchin, *Phys. Rev. D* **68**, 094013 (2003).
- [33] E. Iancu, K. Itakura, and D. N. Triantafyllopoulos, *Nucl. Phys. A* **742**, 182 (2004).
- [34] M. Arneodo, *Phys. Rep.* **240**, 301 (1994).
- [35] A. Accardi, [arXiv:hep-ph/0212148](https://arxiv.org/abs/hep-ph/0212148)
- [36] A. Dumitru, G. Kapilevich, and V. Skokov, *Nucl. Phys. A* **974**, 106 (2018).
- [37] J. Jalilian-Marian and A. H. Rezaeian, *Phys. Rev. D* **85**, 014017 (2012).
- [38] A. H. Rezaeian, *Phys. Lett. B* **718**, 1058 (2013).
- [39] L. McLerran and M. Praszalowicz, *Ann. Phys.* **372**, 215 (2016).
- [40] L. McLerran, *Prog. Theor. Phys. Suppl.* **187**, 17 (2011), High energy strong interactions. Proceedings of the International Symposium, HESI10, Kyoto, Japan, August 9–13, 2010.
- [41] Y. I. Azimov, Y. L. Dokshitzer, V. A. Khoze, and S. I. Troyan, *Z. Phys. C* **27**, 65 (1985).
- [42] K. J. Golec-Biernat and M. Wusthoff, *Phys. Rev. D* **59**, 014017 (1998).
- [43] S. Acharya *et al.* (ALICE collaboration), *Phys. Rev. C* **99**, 024906 (2019).
- [44] B. B. Abelev *et al.* (ALICE collaboration), *Phys. Lett. B* **728**, 25 (2014).
- [45] S. Chatrchyan *et al.* (CMS collaboration), *Eur. Phys. J. C* **72**, 2164 (2012).
- [46] A. M. Sirunyan *et al.* (CMS collaboration), *Phys. Rev. D* **96**, 112003 (2017).
- [47] S. Chatrchyan *et al.* (CMS collaboration), *Eur. Phys. J. C* **74**, 2847 (2014).
- [48] J. Adam *et al.* (ALICE collaboration), *Phys. Lett. B* **760**, 720 (2016).
- [49] M. A. Lisa, S. Pratt, R. Soltz, and U. Wiedemann, *Ann. Rev. Nucl. Part. Sci.* **55**, 357 (2005).
- [50] K. Aamodt *et al.* (ALICE collaboration), *Phys. Rev. D* **84**, 112004 (2011).
- [51] V. Khachatryan *et al.* (CMS collaboration), *J. High Energy Phys.* **05** (2011) 029.
- [52] S. Acharya *et al.* (ALICE collaboration), *Eur. Phys. J. C* **79**, 857 (2019).
- [53] K. Itakura, *Prog. Theor. Phys. Suppl.* **174**, 181 (2008), New frontiers in QCD: Fundamental problems in hot and/or dense matter. Proceedings of the International Workshop and Symposium, YIPQS, Kyoto, Japan, March 3–6, 2008.
- [54] C. Andres, A. Moscoso, and C. Pajares, *Nucl. Phys. A* **901**, 14 (2013).
- [55] S. Acharya *et al.* (ALICE collaboration), *Phys. Rev. C* **101**, 044907 (2020).
- [56] B. Abelev *et al.* (ALICE collaboration), *Phys. Rev. Lett.* **110**, 032301 (2013).

- [57] M. Aaboud *et al.* (ATLAS collaboration), *Phys. Lett. B* **796**, 230 (2019).
- [58] J. Dias de Deus and C. Pajares, *Phys. Lett. B* **695**, 211 (2011).
- [59] M. Braun and C. Pajares, *Phys. Rev. Lett.* **85**, 4864 (2000).
- [60] M. Braun, F. Del Moral, and C. Pajares, *Phys. Rev. C* **65**, 024907 (2002).
- [61] M. Braun and C. Pajares, *Eur. Phys. J. C* **16**, 349 (2000).
- [62] W. Zhang and C. Yang, *J. Phys. G* **41**, 105006 (2014).